

Rationally Designed 3D Hydrogels Model Invasive Lung Diseases Enabling High-Content Drug Screening

Roger Y. Tam, Julien Yockell-Lelièvre, Laura J. Smith, Lisa M. Julian, Alexander E. G. Baker, Chandarong Choey, Mohamed S. Hasim, Jim Dimitroulakos, William L. Stanford,* and Molly S. Shoichet*

Cell behavior is highly dependent upon microenvironment. Thus, to identify drugs targeting metastatic cancer, screens need to be performed in tissue mimetic substrates that allow cell invasion and matrix remodeling. A novel biomimetic 3D hydrogel platform that enables quantitative analysis of cell invasion and viability at the individual cell level is developed using automated data acquisition methods with an invasive lung disease (lymphangioleiomyomatosis, LAM) characterized by hyperactive mammalian target of rapamycin complex 1 (mTORC1) signaling as a model. To test the lung-mimetic hydrogel platform, a kinase inhibitor screen is performed using tuberous sclerosis complex 2 (TSC2) hypomorphic cells, identifying Cdk2 inhibition as a putative LAM therapeutic. The 3D hydrogels mimic the native niche, enable multiple modes of invasion, and delineate phenotypic differences between healthy and diseased cells, all of which are critical to effective drug screens of highly invasive diseases including lung cancer.

Cell invasion is a critical hallmark of metastatic diseases.^[1] There are limited drug therapies that can effectively inhibit both cell invasion and viability of diseased, invasive cells, and when drugs target only one, it can be devastating for the patient. For example, it has been reported that some glioblastoma patients

treated with the anti-VEGF-A (VEGF = vascular endothelial growth factor) monoclonal antibody, bevacizumab, showed increased tumor metastasis despite decreased tumor sizes.^[2] Therefore, drug screening methods that can accurately assess both of these functions are crucial in discovering antimetastatic therapies, yet such screens are lacking. In vitro methods such as transwell plates and Boyden chambers are well established to study cell invasion in response to drug treatments, but these nonphysiological platforms do not provide a biomimetic microenvironment to adequately model cell–matrix interactions involved in the complex mechanisms of cell invasion; they provide detailed information about neither viability nor

invasiveness of individual cells that is necessary to dissect the therapeutic potential of antimetastatic drugs. Moreover, they are incompatible with high throughput screening (HTS).

Cell culture using biomimetic 3D hydrogels is an effective strategy to provide cells with the necessary physical and chemical stimuli to promote native cell growth and function.^[3] Compared to 2D tissue culture on plastic or glass, 3D hydrogels can be remodeled by cells to permit their invasion into the gels. While natural 3D scaffolds (e.g., decellularized extracellular matrix (ECM),^[4] collagen I,^[1a] Matrigel^[5]) have been used to study cell invasion, their physicochemical properties cannot be readily or independently modified to model the ECM of specific diseases. Conversely, synthetic materials can be tuned to mimic the native microenvironment,^[6] but these can be overly simplistic to accurately model native cellular functions. To model cell invasion, protease-degradable synthetic gels have been designed;^[7] however, there are very few gels that permit cells to invade by protease-independent mechanisms.^[8] It is key to model cell invasion by both mechanisms in drug screening of metastatic diseases because clinical trials involving matrix metalloproteinase (MMP) inhibitors alone have historically failed.^[9] Notwithstanding the advantages of using 3D biomaterials to study cell invasion, their application in HTS to identify drugs that inhibit both cellular invasion and viability has been limited,^[10] as most are unsuitable for moderate- to high-throughput screening.


Accurately quantifying both invasion and viability of individual cells remains a challenge in larger drug screens, but

Dr. R. Y. Tam, L. J. Smith, A. E. G. Baker, Prof. M. S. Shoichet
Department of Chemical Engineering and Applied Chemistry
Institute of Biomaterials and Biomedical Engineering
University of Toronto
Toronto, Ontario M5S 3G9, Canada
E-mail: molly.shoichet@utoronto.ca

Dr. R. Y. Tam, Dr. J. Yockell-Lelièvre, Dr. L. M. Julian, C. Choey,
M. S. Hasim, Prof. J. Dimitroulakos, Prof. W. L. Stanford
Ottawa Hospital Research Institute
Regenerative Medicine Program
Ottawa, Ontario K1H 8L6, Canada
E-mail: wstanford@ohri.ca

Prof. W. L. Stanford
Department of Cellular and Molecular Medicine
Ottawa Institute of Systems Biology
University of Ottawa
Ottawa, Ontario K1H 8M5, Canada

Prof. M. S. Shoichet
Department of Chemistry
University of Toronto
Toronto, Ontario M5S 3H6, Canada

 The ORCID identification number(s) for the author(s) of this article can be found under <https://doi.org/10.1002/adma.201806214>.

DOI: 10.1002/adma.201806214

is critical because the increased invasiveness of a few robust surviving cells can be devastating to disease progression, yet difficult to distinguish using assays that rely on homogenous fluorescence detection. The discovery of drugs that inhibit cell invasion is further complicated by the lack of 3D hydrogel platforms that both model the complex mechanisms of cell invasion that occur in cancer metastasis^[1] and discern differences between healthy versus cancer cells.

Recognizing the critical element and complexity of cell invasion to metastatic disease progression and therapeutic intervention, we developed a novel high content, 3D biomimetic hydrogel drug screening platform that permits cell invasion by multiple mechanisms (Figure 1A), and can independently quantify cell viability and invasion at the individual cell level. We demonstrate its utility in screening for compounds that can inhibit these functions in a metastatic and destructive lung disease model, lymphangioleiomyomatosis (LAM), a rare lung neoplasm characterized by: loss of function mutations in tuberous sclerosis complex 1 or 2 (TSC1 or TSC2), the expression of smooth muscle cell (SMC) and neural crest markers, hyperactive mammalian target of rapamycin complex 1 (mTORC1) signaling, and secretion of proteases that remodel and destroy the lung parenchyma.^[11] As primary LAM cells are difficult to proliferate in culture, we have modeled LAM using *TSC2*^{+/-} induced pluripotent stem cell-derived smooth muscle cells (LAM-SMCs), which demonstrate hyperactive mTORC1 signaling and express most LAM cell markers.^[12]

Our 3D hydrogel platform is rationally designed to reflect the ECM of the diseased lung and the complex mechanisms of cell invasion, differentiating it from conventional 2D culture on stiff tissue culture polystyrene (TCPS) (which lacks the ability to be remodeled by invasive cells) and 3D culture using natural biomaterials (which cannot have their physical and chemical properties independently modified). Our hydrogel is composed of hyaluronic acid (HA), which is over-expressed in many invasive cancers,^[13] and binds to the cancer-associated cell surface receptor CD44v6 that is upregulated in LAM^[14] and various cancer cells.^[15]

To form stable HA hydrogels that can withstand the duration of our drug screen, we modified the HA polymer backbone with furan motifs (Figure 1B) that can form stable, covalent chemical bonds with bismaleimide-terminated peptides via Diels-Alder click chemistry (Figure 1C).^[16] The degree of furan modification on HA was quantified by ¹H NMR (Figure S1, Supporting Information), and its presence enables the concentration and composition of maleimide-modified crosslinking and pendant peptides to be customized, which is useful to alter the physical and chemical properties of the hydrogel. As MMPs are secreted by LAM cells,^[17] HA is cross-linked with bismaleimide-terminated collagen-I-derived peptide cross-linkers (GPQG-IWGQ) that can be enzymatically degraded by MMPs, enabling MMP-mediated cell invasion into the hydrogels.

Native lung tissue exhibits viscoelastic behaviors, in which structural deformations of the tissue occur to dissipate energy (i.e., stress relaxation) in response to an applied stress force. This occurs via the reorganization of collagen and elastin fibers that comprise the lungs.^[18] Thus, we include a second polymer with well-characterized viscoelastic properties (methylcellulose) into our 3D hydrogel system that can form weak, reversible physical crosslinks (via hydrophobic interactions between the methoxy groups of the polysaccharide backbone) to permit

cultured cells to remodel the material. To ensure that methylcellulose is retained for the duration of our assay, we chemically modified methylcellulose with reactive thiols (MC-SH, 5% degree of substitution) that form chemical crosslinks with maleimide-functionalized peptides via conjugate Michael addition chemistry (Figure 1B,C). Inclusion of MC-SH into the hydrogel platform increased stress relaxation, but did not significantly affect Young's modulus, as determined by unconfined compression testing (Figure 1D,E). We further compared the mechanical properties of these hydrogels (which we optimized to enable cell invasion) to that of the rat lung (1.10 ± 0.20 kPa for HA-MMP cross-linked hydrogel vs 5.54 ± 2.55 kPa for rat lung tissue, Figure S2, Supporting Information), both of which are within the range of other reports of native human lung tissue (1–5 kPa),^[19] and orders of magnitude lower than conventional 2D TCPS (>1 GPa).

To further enhance cell interaction with the matrix through other cancer-associated integrin receptors expressed on the cell surface (i.e., integrins $\alpha v \beta 3$),^[20] we immobilized the corresponding ligand (i.e., vitronectin peptide, maleimide-PQVTRG-DVFTMP)^[21] into the gels via conjugation to the unreacted furans in the HA backbone.

The hyaluronan hydrogel-based platform favors cell invasion of *TSC2*^{+/-} LAM-SMCs (Figure 1F) over healthy *TSC2*^{+/+} control SMCs, thereby reflecting what is observed clinically (Figure 1G). To gain greater insight into how our hydrogels can be used to study cell invasion mechanisms such as MMP-dependent and independent pathways, we characterized several aspects of cellular invasion using pharmacological treatment and varying composition of our 3D hydrogel. Using standard gelatin zymography, we detected increased levels of MMP9 secreted by LAM-SMCs compared to control SMCs and transformed angiomyolipoma (*TSC2*^{-/-}) cells (which exhibit a subset of LAM-associated phenotypes). Similarly, LAM-SMCs increased MMP2 compared to *TSC2*^{-/-} angiomyolipoma cells (Figure 1H and Figure S3, Supporting Information). The small amount of MMP2 detected in the media-only control is attributed to the presence of 1% fetal bovine serum (FBS) used in the culture media.^[22] These data demonstrate that our 3D hydrogels differentiate the MMP-dependent invasive behaviors between patient-derived LAM-SMCs, control SMCs, and the angiomyolipoma *TSC2*^{-/-} cell line, further validating this model to study LAM. Moreover, treatment of the invasive LAM-SMCs with the pan MMP inhibitor (GM6001, 10×10^{-6} M) resulted in modest, yet statistically significant decrease in cell invasion (Figure 1I), suggesting that mechanisms other than MMP secretion alone mediate invasion.

We questioned whether MMP-independent mechanisms are required for LAM-SMC hydrogel invasion given that viscoelastic matrices, which can be remodeled or deformed (by stress-relaxation), increase cell mobility and adhesion compared to elastic matrices.^[3c,23] We show that LAM-SMCs, but not control cells, exhibit increased invasion ($p < 0.001$) in the presence (vs absence) of the viscoelastic polymer MC-SH (Figure 1J), which has increased stress relaxation.

To further assess MMP-independent cell invasion into our 3D hydrogels, cells were treated with the Src inhibitor, Saracatinib, and the Rho-associated protein kinase (ROCK) inhibitor, Y-27632 (Figure 1K). Src kinase, in conjunction with

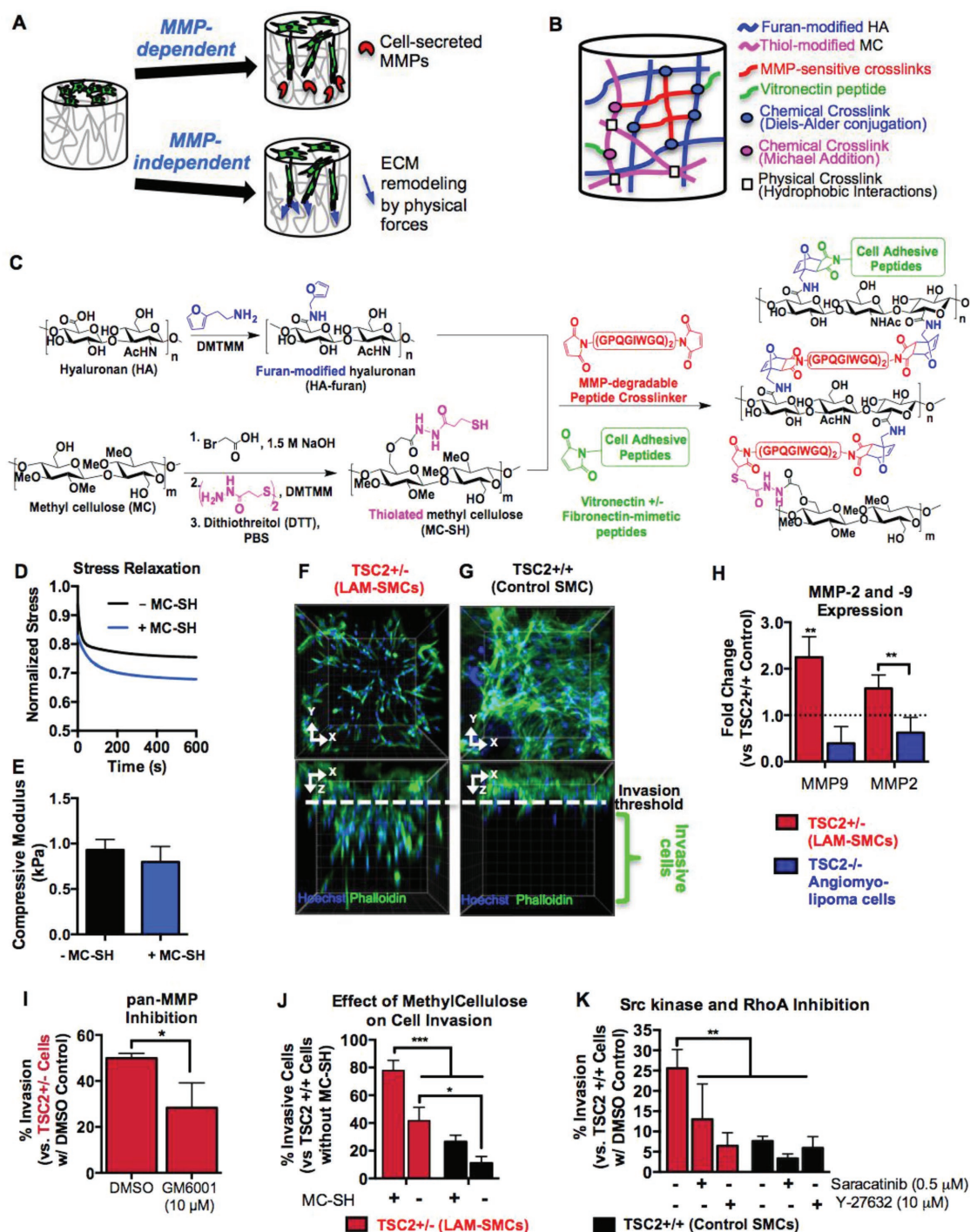


Figure 1. *TSC2*^{+/-} LAM-SMCs invade 3D MMP-degradable HA hydrogels via MMP-dependent and -independent mechanisms. **A)** Schematic representation of potential cell invasion mechanisms. **B)** Schematic representation of the composition of biomimetic stimuli-responsive 3D HA hydrogels. **C)** Synthetic scheme describing the synthesis of HA-furan/MC-SH hydrogels cross-linked with MMP-degradable peptides, and immobilized with cell-adhesive peptides. **D)** Stress relaxation of HA-furan/MMP hydrogels is increased with thiolated methylcellulose (MC-SH, blue) compared to gels without MC-SH (black). **E)** Compressive Modulus of hydrogels with or without 0.5 mg mL⁻¹ MC-SH are not statistically different. *N* = 4. Mean + SD. **F)** *TSC2*^{+/-} LAM-smooth muscle cells (LAM-SMCs) isolated from patient-derived iPSCs cultured on biomimetic 3D hyaluronan (HA)-based hydrogels are more invasive than **G)** iPSC-derived *TSC2*^{+/+} control SMCs. **H)** MMP-2 and MMP-9 expression in invasive *TSC2*^{+/-} LAM-SMCs (red bars) relative to *TSC2*^{+/+} cells (dashed line) and *TSC2*^{-/-} angiomyolipoma cells (blue bars), assessed by zymography of conditioned media isolated from the various cell types. *N* = 3, ****p* < 0.01 represents a significant difference from *TSC2*^{+/+} control SMCs and *TSC2*^{-/-} angiomyolipoma cells for MMP9, and a significant difference between *TSC2*^{+/-} LAM-SMCs and *TSC2*^{-/-} angiomyolipoma cells for MMP2. **I)** GM6001 partially inhibits invasion of *TSC2*^{+/-} LAM-SMCs into 3D hydrogels. *N* = 3, **p* < 0.05. **J)** Hydrogels lacking thiolated methylcellulose (MC-SH) show decreased invasion of each cell type. *N* = 3. **K)** Treatment with saracatinib or Y-27632 decrease cell invasion. *N* = 4. For (J,K): **p* < 0.05, ***p* < 0.01, ****p* < 0.001.

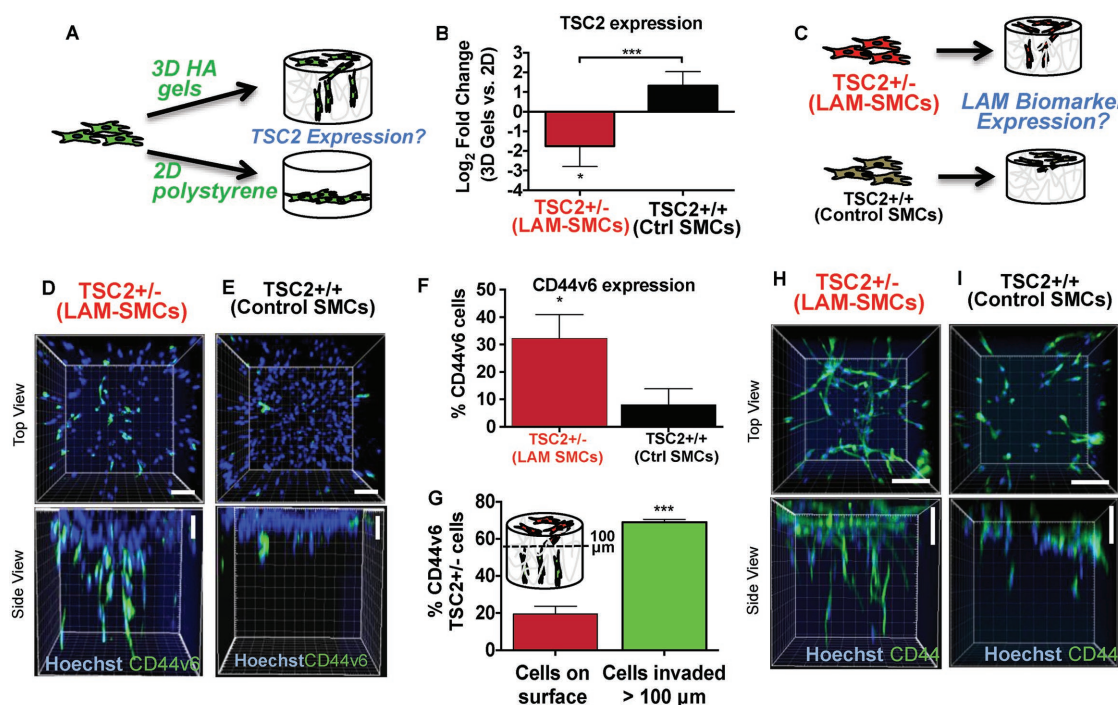


Figure 2. Patient-derived ($TSC2^{+/-}$) LAM-SMCs exhibit LAM-like characteristics when cultured in 3D HA hydrogels. A) Schematic representation showing cells cultured on 2D polystyrene versus 3D hydrogels. B) Patient-derived ($TSC2^{+/-}$) LAM-SMCs express lower levels of $TSC2$ when cultured on 3D HA gels versus on 2D polystyrene. Conversely, $TSC2^{+/+}$ control SMCs express higher levels of $TSC2$ when cultured on 3D HA gels versus 2D polystyrene. $N = 4$. $*p < 0.05$, $**p < 0.01$ indicates significant differences between each respective cell type cultured on 3D versus 2D (horizontal line). $***p < 0.001$ indicates significant difference between $TSC2^{+/+}$ control SMCs and $TSC2^{+/-}$ LAM-SMCs cultured on 3D gels. C) Schematic representation depicting the culture of $TSC2^{+/-}$ LAM-SMCs versus $TSC2^{+/+}$ control SMCs on 3D HA hydrogels. D,E) Representative confocal images showing the expression of CD44v6 (green, anti-CD44v6). Blue is Hoechst (for nuclei). Scale bar represents 100 μm . F) Patient-derived $TSC2^{+/-}$ LAM-SMCs cultured on 3D HA hydrogels express higher levels of CD44v6 versus $TSC2^{+/+}$ control SMCs. G) Schematic and quantification of CD44v6 expression of invasive ($>100 \mu\text{m}$) versus noninvasive ($<100 \mu\text{m}$) cells. For (F,G): $N = 3$, $*p < 0.05$, $***p < 0.001$. H, I) Representative confocal images demonstrate expression of the hyaluronan receptor CD44 (green, anti-CD44) on both (H) $TSC2^{+/-}$ LAM-SMCs and (I) $TSC2^{+/+}$ control SMCs.

integrin $\beta 1$ upregulation, is critical for invadopodia formation in MMP-independent cell invasion through the ECM.^[1b,24] Saracatinib ($0.5 \times 10^{-6} \text{ M}$) significantly decreased the relative percentage of invasive LAM-SMCs compared to DMSO-treated controls (Figure 1K) while not significantly affecting MMP9 secretion or cell viability ($p > 0.05$, Figure S4A,B, Supporting Information), demonstrating MMP-independent cell invasion. RhoA activation of cytoskeletal contraction is another MMP-independent mechanism.^[1b] Interestingly, LAM- and control-SMCs treated with Y-27632, an inhibitor of ROCK, significantly decreased cell invasion ($p < 0.01$, Figure 1K), although neither cell viability nor MMP9 secretion levels of LAM-SMCs were affected ($p > 0.05$, Figure S4C,D, Supporting Information). This further substantiates that MMP-independent mechanisms also contribute to LAM cell invasion.

Together, HA and MC polysaccharides form a stable hydrogel for cell-mediated invasion that is both MMP-dependent—by degradation of MMP-cleavable crosslinks between HA chains, and MMP-independent—by physical displacement of reversible hydrophobic interactions between MC chains.

Immunocytochemistry of LAM lesions^[25] suggests that in addition to $TSC2^{-/-}$ cells, $TSC2^{+/-}$ SMCs play a pathophysiological role in LAM lesions. We determined how $TSC2$ gene expression is affected by the substrate on which the cells are cultured and hypothesized that $TSC2^{+/-}$ LAM-SMCs cultured

in our biomimetic hydrogel would behave more similarly to in vivo LAM cells. We previously reported that $TSC2^{+/-}$ LAM-SMCs express decreased levels of $TSC2$ at both mRNA and protein levels compared to $TSC2^{+/+}$ control SMCs when cultured on 2D TCPS.^[12] To assess the impact of cell-substrate interactions, we quantified $TSC2$ levels by performing qRT-PCR of patient-derived $TSC2^{+/-}$ LAM-SMCs and $TSC2^{+/+}$ control SMCs cultured on either stiff 2D TCPS or soft biomimetic 3D HA hydrogels (Figure 2A,B). LAM-SMCs cultured on 3D HA hydrogels express decreased $TSC2$ transcript compared to those cultured on 2D TCPS ($p < 0.01$). Surprisingly, $TSC2^{+/+}$ control SMCs increased $TSC2$ mRNA levels when cultured on 3D hydrogels compared to 2D ($p < 0.05$), revealing an even greater difference between control and patient-derived LAM-SMCs in our biomimetic 3D HA hydrogels than on 2D TCPS ($p < 0.001$), thereby highlighting the importance of growing cells in tissue-mimetic 3D conditions to model disease.

To gain insight into the interactions between the 3D HA matrix and cells cultured therein, we assessed the cell surface abundance of CD44 and CD44v6 receptors that naturally bind to HA and are upregulated in many cancer cells,^[26] including primary cells isolated from the lungs of LAM patients (Figure 2C).^[14] $TSC2^{+/-}$ LAM-SMCs showed markedly increased expression of a variant of CD44 that is associated with LAM and cancer cell invasion (CD44v6) compared to control SMCs (Figure 2D–F,

$p < 0.05$), consistent with immunohistochemistry of primary LAM nodules. We quantified the degree of CD44v6⁺ cells based on their invasiveness into the hydrogels (Figure 2G): cells that invade greater than a depth of 100 μm show increased CD44v6 expression compared to noninvasive cells (Figure 2D,G, $p < 0.001$), further demonstrating the importance of this cell-surface marker as an indicator of invasiveness of LAM cells. Unlike CD44v6, CD44 is expressed in iPSC-derived SMCs of both LAM patients and normal controls regardless of their invasiveness (Figure 2H,I).

We demonstrate the role of vitronectin in our hydrogel platform by first confirming that LAM-SMCs express higher levels of the vitronectin-interacting integrin subunits αV , β1 , and β3 compared to control SMCs (Figure S5A–I, Supporting Information). By varying vitronectin concentrations, we observe that an optimal vitronectin peptide concentration of 25×10^{-6} M promotes the greatest differences in cell invasion between LAM and control SMCs (Figure S6, Supporting Information). While the overall percentage of invasive cells is comparable between hydrogels immobilized with 0, 25 or 250×10^{-6} M of vitronectin peptide ($p > 0.05$, Figure S6B, Supporting Information), we observe the greatest statistical differences in the number of invasive cells between the two cell types at 25×10^{-6} M compared to 0 and 250×10^{-6} M ($p < 0.0001$, $p < 0.05$, $p < 0.01$ for 25, 0, 250×10^{-6} M, respectively, Figure S6C, Supporting Information). The absence of vitronectin peptide results in an overall decrease in cell number for LAM-SMCs, and consequently a decrease in the number of invasive cells ($p < 0.05$, Figure S6C, Supporting Information). Conversely, both LAM and control SMCs cultured on gels with the highest peptide concentration (1000×10^{-6} M) formed monolayers on top of the gels (Figure S6C,I,M, Supporting Information) with minimal invasion.

To gain further insight into the differences between the percentage and number of invasive cells (Figure S6B,C, Supporting Information) at 0 and 25×10^{-6} M, we studied the viability (Figure S7, Supporting Information) of cells cultured in hydrogels immobilized with 0, 25, 250, and 1000×10^{-6} M of vitronectin peptide. We observed that while cell proliferation (Ki 67⁺ cells) is not statistically different between cells grown in 0 to 1000×10^{-6} M vitronectin, the lack of peptide resulted in decreased cell viability (Calcein AM[−] staining) and increased early and late apoptosis (Annexin V⁺ and propidium iodide (PI)⁺ cells, respectively) of LAM SMCs. Therefore, with our goal in using a hydrogel system as a platform that can delineate differences in cell invasion between LAM and control SMCs for drug screening applications, we performed subsequent drug screening experiments for both cell viability and invasion using 25×10^{-6} M.

To test whether our hydrogel platform is optimized for performing high-content drug screening of cell invasion and viability, we compared our strategy to previously reported methods used to study LAM cell invasion, such as cell culture in conventional collagen I hydrogels and the use of angiomyolipoma ($TSC2^{-/-}$) cells.^[11a,27] In comparison to collagen I, we observed a greater difference in our HA hydrogels between $TSC2^{-/-}$ LAM-SMCs and $TSC2^{+/+}$ control SMCs (Figure S8, Supporting Information). Surprisingly, both cell types showed significantly greater invasion compared to $TSC2^{-/-}$ angiomyolipoma cells ($p < 0.01$, Figure S9, Supporting

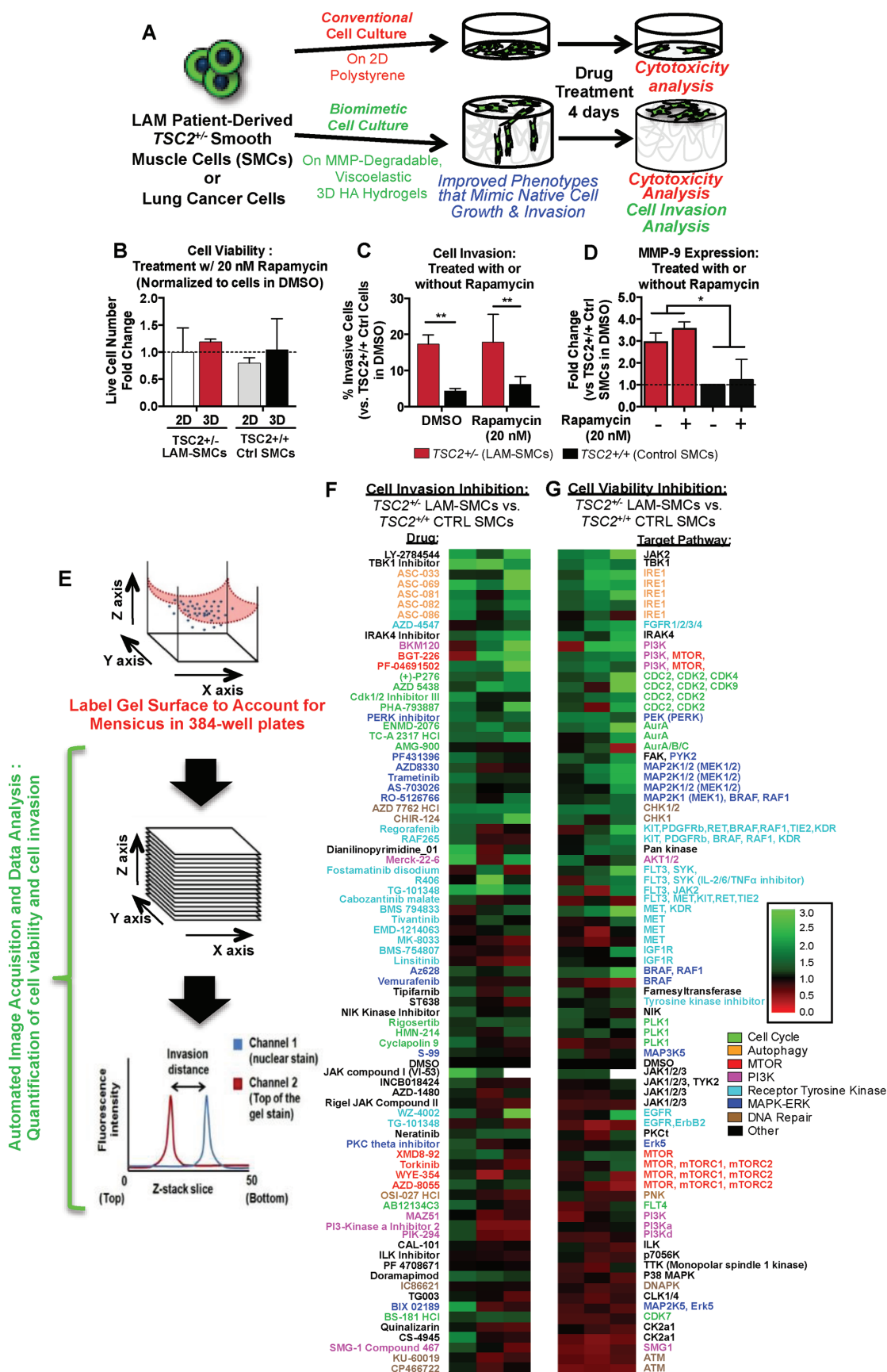
Information), reflecting the superiority of both our hydrogel and cells to model LAM.

For invasive diseases, both cell viability and invasion are key outcome measures of drug therapies. Currently, the only approved therapeutic treatment for LAM is the mTORC1 inhibitor rapamycin,^[28] which slows the decline in lung performance of LAM patients, but as a cytostatic and not cytotoxic agent, rapamycin has limited effectiveness. Upon withdrawal of rapamycin, lung function decreases comparably to placebo-treated control patients, emphasizing the need to discover more efficacious drugs. We tested the efficacy of rapamycin in our 3D hydrogel platform: treatment with rapamycin at 20×10^{-9} M (and up to 1×10^{-6} M) had little effect on the viability of either patient-derived $TSC2^{-/-}$ LAM-SMCs or $TSC2^{+/+}$ control SMCs (Figure 3A,B) cultured on either 2D TCPS or 3D gels, thereby corroborating the patient data.^[27,28] Moreover, rapamycin treatment neither diminished cell invasion of LAM-SMCs (Figure 3C, $p = 0.998$) nor decreased MMP expression (Figure 3D, $p = 0.543$).

Next, we incorporated our hydrogel into a drug-screening platform and tested drug response between $TSC2^{-/-}$ LAM-SMCs and healthy $TSC2^{+/+}$ control SMCs. We modified our culture system to a 384-well format to enable higher throughput screening and simultaneous quantification of cell invasion and cell viability. At the endpoint of the assay (4 days), cell viability is determined by staining with both Hoechst (for cell nuclei) and SYTOX Green (for dead cells) while cell invasion is measured by automated confocal imaging: the hydrogel surface is demarcated using silica gel particles to accurately account for the gel-surface meniscus present in 384-well plates and z-stacked images are obtained for each well using an automated confocal high content imaging system (Figure 3E). We developed a novel algorithm in ImageJ to quantify cell invasion from the surface of the hydrogels by subtracting the Z-position of the cell nuclei from the Z-position of silica gel particles (i.e., at the gel surface) at the same XY coordinates. Together with identification of dead cells by staining with SYTOX Green, this method enables independent quantification of viability and invasion of individual cells (Figure S10, Supporting Information).

We used our 3D hydrogel platform to simultaneously and independently assess cell invasion and viability of a panel of 80 kinase inhibitors (Figure 3F,G), thereby identifying potential drug candidates and target pathways toward $TSC2^{-/-}$ LAM-SMCs versus $TSC2^{+/+}$ control SMCs. Treatment with drugs that showed selective decrease in both cell viability and invasion toward LAM-SMCs (denoted by green in the heat map, Figure 3F,G) include those that affect: 1) cell cycle—, i.e., cyclin-dependent kinase inhibitors: Cdk1/2 inhibitor, PHA-793887, AZD5438, and (+)–P276; Aurora A inhibitors: ENMD-2076, TC-A 2317 HCl; and 2) autophagy—, i.e., IRE1 inhibitors: ASC-033, ASC-069, ASC-081, ASC-082, and ASC-086, indicating that these specific pathways represent pharmacological targets in pulmonary LAM. Surprisingly, drugs that directly targeted the mTOR pathway (which is downstream of TSC2) did not consistently inhibit both invasion and viability of hypomorphic $TSC2^{-/-}$ LAM-SMCs, suggesting the importance of targeting mTORC1-independent pathways in LAM.

To test the broad utility of our hydrogel platform, multiple lung cancer cells were cultured on our HA hydrogels



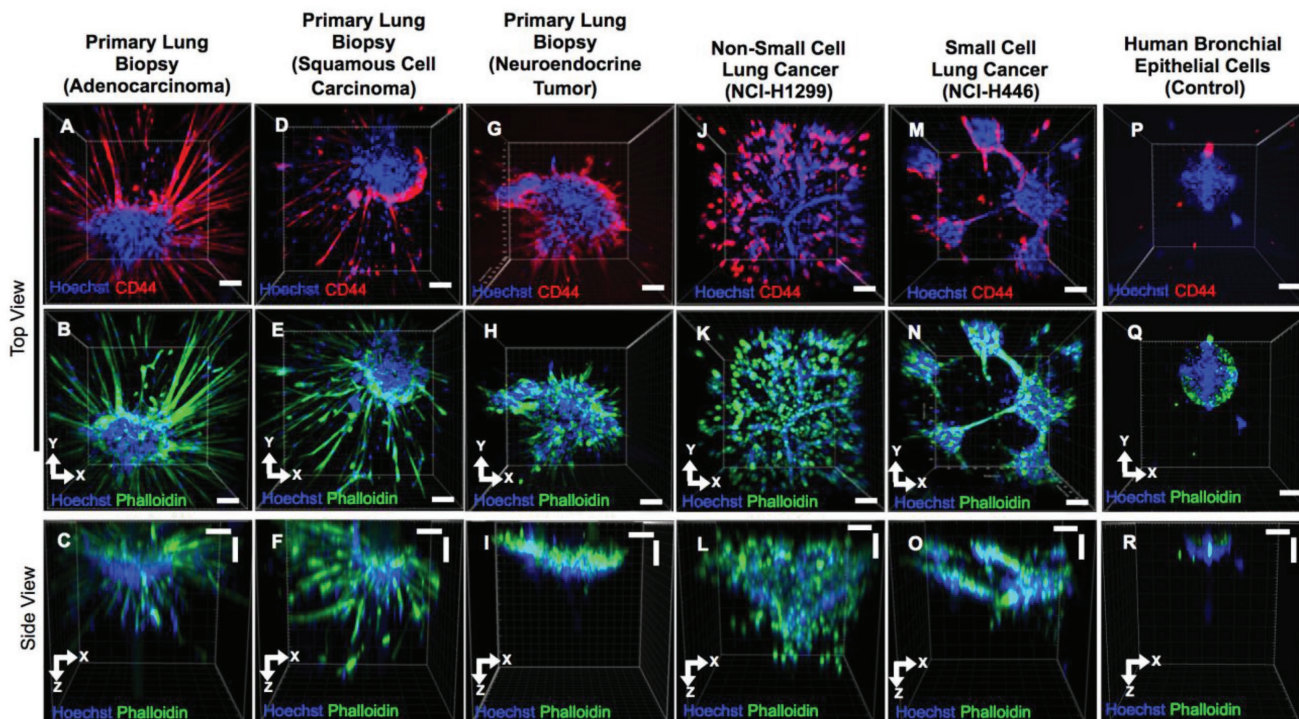


Figure 4. Lung cancer cells express CD44 and show varying invasiveness into 3D HA hydrogels. A–I) Primary cells isolated and cultured from three separate lung carcinoma biopsies identified as (A–C) adenocarcinoma, (D–F) squamous cell carcinoma, and (G–I) neuroendocrine tumor. J–L) Non-small cell lung cancer (NCI-H1299) and M–O) small cell lung cancer (NCI-H446) cells. P–R) Healthy human bronchial epithelial control cells do not invade into 3D hydrogels. (A,D,G,I,M) Lung cancer cells express CD44, while (P) healthy bronchial epithelial cells do not.

(Figure 4A–O). Three distinct patient-derived primary lung cancer cell preparations, isolated from three separate lung cancer tissue biopsies and identified as adenocarcinoma (Figure 4A–C), squamous cell carcinoma (Figure 4D–F), and neuroendocrine tumor (Figure 4G–I), along with commercially available human non-small cell lung cancer (NSCLC, NCI-H1299, Figure 4J–L) and small cell lung cancer (SCLC, NCI-H446) cells (Figure 4M–O) all express CD44 (Figure 4A,D,G,J,M and Figure S11, Supporting Information), which is the natural ligand for HA. Interestingly, CD44 is predominantly expressed on cells that are at the cell–matrix interface (i.e., on the outside of multicellular cell clusters and on single cells), yet is not readily detected in cells within the cell clusters, consistent with this receptor interacting with the HA hydrogel. However,

healthy human bronchial epithelial control cells do not express CD44 (Figure 4P), further highlighting the advantage of using HA-based hydrogels to culture lung cancer cells.

Confocal imaging analysis revealed different cell morphologies and levels of invasiveness, which cannot be assessed with conventional 2D cell culture or Boyden chamber/transwell assays. Cells isolated and cultured from three lung biopsies formed large cell clusters with spindle-like cells migrating away from these clusters; however, only cells from adenocarcinoma and squamous cell carcinoma biopsies showed high degrees of cell invasion (Figure 4C,F), whereas cells grown from a neuroendocrine biopsy showed less invasion (Figure 4I). Interestingly, non-small cell lung cancer (NCI-H1299) cells grew and invaded as single cells (Figure 4K,L), whereas SCLC cells formed interconnected

Figure 3. 3D biomimetic in vitro model of LAM and application to automated analysis of cell invasion and viability. A) TSC2^{+/−} LAM-smooth muscle cells (LAM-SMCs) isolated from patient-derived iPSCs cultured on biomimetic 3D hyaluronan (HA)-based hydrogels enable cells to recapitulate their native growth compared to conventional culture on 2D tissue culture polystyrene. 3D cell culture allows drugs to be screened for cell viability and invasion. B–D) Response of LAM-SMCs and control SMCs treated with 20×10^{-9} M rapamycin (mTORC1 inhibitor), the only clinically approved therapy for LAM. B) Viability of cells cultured on 2D and 3D HA gels, normalized to cells cultured on the same substrate treated with DMSO (dotted line). C) Cell invasion into 3D HA gels. ($N = 4$, $**p < 0.01$). D) Active MMP-9 expression, assessed by zymography of conditioned media. ($N = 3$, $*p < 0.05$). E) Schematic representation of algorithm used to automatically quantify cell invasion using an ImageJ macro. The gel surface is demarcated with silica particles, and Z-stack images are captured for each channel; the XYZ coordinate of each cell is identified, and at each cellular XY coordinate, the distance of cell invasion is equal to the difference between the maximum signal along the Z-axis of the gel surface marker (red curve) and the cell (blue curve). F,G) Heat maps showing the inhibition of average cell invasion (F) and cell viability (G) of LAM-SMCs versus control SMCs treated with 80 kinase inhibitor drugs (at 5×10^{-6} M). Green boxes within the heat map indicate greater selectivity and efficacy in terms of reduced invasion and viability of LAM-SMCs versus control SMCs, while red boxes indicate the opposite (and undesirable) drug response. The order of the drug names in (F) corresponds to their respective target pathway listed in (G). Columns represent biological replicates. Selected target pathways or cell functions are color-coded (Green = cell cycle; orange = autophagy; red = MTOR, magenta = phosphoinositide-3 kinase (PI3K) pathway; turquoise = receptor tyrosine kinase; blue = MAPK-ERK pathway; brown = DNA repair; black = other).

multicellular spheroids from which single cells also invade into the hydrogels (Figure 4N,O). In contrast, healthy bronchial epithelial control cells do not invade and instead remain on the surface of these hydrogels as spherical aggregates (Figure 4Q,R).

In summary, the modular design of our hydrogel system enables its physicochemical properties to be readily tuned to model disease and tissue-specific ECMs by independently modifying its biochemical composition, matrix stiffness, and viscoelasticity. We hypothesize that this will allow other metastatic diseases involving tissue remodeling and invasion by protease-dependent and -independent mechanisms to be emulated. We demonstrate the breadth of our hydrogel platform to study LAM and lung cancer by culturing both primary human lung cancer cells and commercially available lung cancer cells. These cancer cells invade into our hydrogels whereas healthy human bronchial epithelial cells do not, highlighting the application of our hydrogel platform to other diseases in addition to LAM.

Our platform, using the 384-well plate format with automated image acquisition and data analysis, can be readily scaled up using chemical synthesis and used by liquid handling automation to perform larger drug screens. With the ability to monitor invasion and viability at the individual cell level, more detailed analyses of cellular responses to drug treatments are possible, allowing for greater predictive capacity for efficacy than current strategies in drug discovery of antimetastatic therapeutics.

Supporting Information

Supporting Information is available from the Wiley Online Library or from the author.

Acknowledgements

The authors thank Catherine Lawrence for her inspiration, and members of the Shoichet and Stanford Labs for thoughtful review of this paper. Funding: The authors thank the Canadian Institute of Health Research (CIHR) and Natural Sciences and Engineering Research Council of Canada (NSERC) for financial support through the Collaborative Health Research Program (MSS), and Tier 1 Canada Research Chair Program in Integrative Stem Cell Biology (WLS) and in Tissue Engineering (MSS). This research was supported by a Special Accelerated Discovery grant by the McEwen Centre for Regenerative Medicine, supported by Green Eggs and LAM (WLS and MSS), a LAM Foundation Pilot grant (LAM0123P01-17 to WLS) and the United States Department of Defense via the Tuberous Sclerosis Complex Research Program of the Congressionally Directed Medical Research Program (W81XWH-14-1-0434 to WLS). L.J.S. and A.E.G.B. acknowledge support from NSERC (PGSD and CGSD, respectively), and L.M.J. is supported by CIHR Banting and Ontario Institute of Regenerative Medicine Postdoctoral Fellowships. The authors thank Stephanie Fisher for assisting with mechanical testing. The authors acknowledge the Canadian Foundation for Innovation, project number 19119, and the Ontario Research Fund for funding of the Centre for Spectroscopic Investigation of Complex Organic Molecules and Polymers. Primary lung cancer cells were obtained from patient lung tumor tissues collected upon resection (lobectomy) following patient consent (Ottawa Hospital Research Ethics Board; Protocol # 20120559-01H).

Conflict of Interest

The authors declare they have no competing interests, yet a patent has been submitted.

Keywords

3D hydrogels, cancer, cell invasion, disease modeling, drug screening

Received: September 25, 2018

Revised: November 9, 2018

Published online:

- [1] a) F. Sabeh, R. Shimizu-Hirota, S. J. Weiss, *J. Cell Biol.* **2009**, *185*, 11; b) P. Friedl, K. Wolf, *Nat. Rev. Cancer* **2003**, *3*, 362.
- [2] J. F. de Groot, G. Fuller, A. J. Kumar, Y. Piao, K. Eterovic, Y. Ji, C. A. Conrad, *Neuro-Oncology* **2010**, *12*, 233.
- [3] a) M. J. Bissell, D. C. Radisky, A. Rizki, V. M. Weaver, O. W. Petersen, *Differentiation* **2002**, *70*, 537; b) C. Yang, M. W. Tibbitt, L. Basta, K. S. Anseth, *Nat. Mater.* **2014**, *13*, 645; c) O. Chaudhuri, L. Gu, M. Darnell, D. Klumpers, S. A. Bencherif, J. C. Weaver, N. Huebsch, D. J. Mooney, *Nat. Commun.* **2015**, *6*, 6364.
- [4] A. Glentis, P. Oertle, P. Mariani, A. Chikina, F. El Marjou, Y. Attieh, F. Zaccarini, M. Lae, D. Loew, F. Dingli, P. Sirven, M. Schoumacker, B. G. Gurchenkov, M. Plodinec, D. M. Vignjevic, *Nat. Commun.* **2017**, *8*, 924.
- [5] O. W. Petersen, L. Ronnov-Jessen, A. R. Howlett, M. J. Bissell, *Proc. Natl. Acad. Sci. U. S. A.* **1992**, *89*, 9064.
- [6] S. R. Calia, J. A. Burdick, *Nat. Methods* **2016**, *13*, 405.
- [7] a) S. A. Fisher, R. Y. Tam, A. Fokina, M. M. Mahmoodi, M. D. Distefano, M. S. Shoichet, *Biomaterials* **2018**, *178*, 751; b) J. Patterson, J. A. Hubbell, *Biomaterials* **2010**, *31*, 7836.
- [8] M. Ehrbar, A. Sala, P. Lienemann, A. Ranga, K. Mosiewicz, A. Bittermann, S. C. Rizzi, F. E. Weber, M. P. Lutolf, *Biophys. J.* **2011**, *100*, 284.
- [9] A. Winer, S. Adams, P. Mignatti, *Mol. Cancer Ther.* **2018**, *17*, 1147.
- [10] a) H. A. Kenny, M. Lal-Nag, E. A. White, M. Shen, C. Y. Chiang, A. K. Mitra, Y. Zhang, M. Curtis, E. M. Schryver, S. Bettis, A. Jadhav, M. B. Boxer, Z. Li, M. Ferrer, E. Lengyel, *Nat. Commun.* **2015**, *6*, 6220; b) N. A. Evensen, J. Li, J. Yang, X. Yu, N. S. Sampson, S. Zucker, J. Cao, *PLoS One* **2013**, *8*, e82811; c) Y. Fang, R. M. Eglén, *SLAS Discovery* **2017**, *22*, 456.
- [11] a) T. N. Darling, G. Pacheco-Rodriguez, A. Gorio, E. Lesma, C. Walker, J. Moss, *Lymphatic Res. Biol.* **2010**, *8*, 59; b) E. P. Henske, F. X. McCormack, *J. Clin. Invest.* **2012**, *122*, 3807.
- [12] L. M. Julian, S. P. Delaney, Y. Wang, A. A. Goldberg, C. Dore, J. Yockell-Lelievre, R. Y. Tam, K. Giannikou, F. McMurray, M. S. Shoichet, M. E. Harper, E. P. Henske, D. J. Kwiatkowski, T. N. Darling, J. Moss, A. S. Kristof, W. L. Stanford, *Cancer Res.* **2017**, *77*, 5491.
- [13] C. J. Whatcott, H. Han, R. G. Posner, G. Hostetter, D. D. Von Hoff, *Cancer Discovery* **2011**, *1*, 291.
- [14] G. Pacheco-Rodriguez, W. K. Steagall, D. M. Crooks, L. A. Stevens, H. Hashimoto, S. Li, J. A. Wang, T. N. Darling, J. Moss, *Cancer Res.* **2007**, *67*, 10573.
- [15] S. Misra, V. C. Hascall, R. R. Markwald, S. Ghatak, *Front. Immunol.* **2015**, *6*, 201.
- [16] S. C. Owen, S. A. Fisher, R. Y. Tam, C. M. Nimmo, M. S. Shoichet, *Langmuir* **2013**, *29*, 7393.
- [17] M. K. Glassberg, S. J. Elliot, J. Fritz, P. Catanuto, M. Potier, R. Donahue, W. Stetler-Stevenson, M. Karl, *J. Clin. Endocrinol. Metab.* **2008**, *93*, 1625.
- [18] B. Suki, J. H. Bates, *Respir. Physiol. Neurobiol.* **2008**, *163*, 33.
- [19] A. J. Booth, R. Hadley, A. M. Cornett, A. A. Dreffs, S. A. Matthes, J. L. Tsui, K. Weiss, J. C. Horowitz, V. F. Fiore, T. H. Barker, B. B. Moore, F. J. Martinez, L. E. Niklason, E. S. White, *Am. J. Respir. Crit. Care Med.* **2012**, *186*, 866.
- [20] M. Y. Hsu, D. T. Shih, F. E. Meier, P. Van Belle, J. Y. Hsu, D. E. Elder, C. A. Buck, M. Herlyn, *Am. J. Pathol.* **1998**, *153*, 1435.

- [21] S. Suzuki, A. Oldberg, E. G. Hayman, M. D. Pierschbacher, E. Ruoslahti, *EMBO J.* **1985**, 4, 2519.
- [22] X. Hu, C. Beeton, *J. Visualized Exp.* **2010**, 45, 2445.
- [23] A. R. Cameron, J. E. Frith, G. A. Gomez, A. S. Yap, J. J. Cooper-White, *Biomaterials* **2014**, 35, 1857.
- [24] a) K. C. Williams, M. G. Coppelino, *J. Cell Sci.* **2014**, 127, 1712; b) C. Albiges-Rizo, O. Destaing, B. Fourcade, E. Planus, M. R. Block, *J. Cell Sci.* **2009**, 122, 3037.
- [25] D. Clements, A. Dongre, V. P. Krymskaya, S. R. Johnson, *PLoS One* **2015**, 10, e0126025.
- [26] a) C. Underhill, *J. Cell Sci.* **1992**, 103, 293; b) K. H. Heider, H. Kuthan, G. Stehle, G. Munzert, *Cancer Immunol. Immunother.* **2004**, 53, 567.
- [27] C. Li, P. S. Lee, Y. Sun, X. Gu, E. Zhang, Y. Guo, C. L. Wu, N. Auricchio, C. Priolo, J. Li, A. Csibi, A. Parkhitko, T. Morrison, A. Planaguma, S. Kazani, E. Israel, K. F. Xu, E. P. Henske, J. Blenis, B. D. Levy, D. Kwiatkowski, J. J. Yu, *J. Exp. Med.* **2014**, 211, 15.
- [28] F. X. McCormack, Y. Inoue, J. Moss, L. G. Singer, C. Strange, K. Nakata, A. F. Barker, J. T. Chapman, M. L. Brantly, J. M. Stocks, K. K. Brown, J. P. Lynch 3rd., H. J. Goldberg, L. R. Young, B. W. Kinder, G. P. Downey, E. J. Sullivan, T. V. Colby, R. T. McKay, M. M. Cohen, L. Korbee, A. M. Taveira-DaSilva, H. S. Lee, J. P. Krischer, B. C. Trapnell, National Institutes of Health Rare Lung Diseases Consortium, MILES Trial Group, *N. Engl. J. Med.* **2011**, 364, 1595.